Entropy Field Decomposition Analysis of Atmospheric River Formation

Lawrence R. Frank[1], **Vitaly L. Galinsky**[1], **Zhenhai Zhang**[2], **and F. Martin Ralph**[2]

[1]UCSD Center for Scientific Computation in Imaging
[2]UCSD Center for Western Weather and Water Extremes

Key Points:

- The entropy field decomposition (EFD) can detect atmospheric rivers (ARs) directly from coupled wind and specific humidity fields.
- Space-time information trajectories (STITs) generated from EFD modes reveal a link between ARs and planetary-scale circulation.
- EFD provides a general framework for analyzing spatiotemporal modes of complex non-linear systems including interacting fields such as ARs.

Corresponding author: Lawrence R. Frank, lfrank@ucsd.edu

Abstract
A novel method for estimating spatial-temporal modes of time varying data containing complex non-linear interacting multivariate fields, called the entropy field decomposition (EFD), is applied to the problem of characterizing the formation and intensification of atmosphere rivers (ARs), and reveals two novel findings. First, analysis of global time-varying interacting wind (w) and specific humidity (q) fields produces spatiotemporal modes consistent with observed global distribution of ARs detected by Integrated Water Vapor Transport (IVT). Secondly, space-time information trajectories (STITs) generated from coupled w-q EFD modes, representing optimal (in the sense of maximum entropy) parameter pathways, reveal a clear connection between ARs and planetary-scale circulation with structure similar to Rossby waves and reveal that ARs appear to be dynamically linked with the outflow region of the wave troughs. These findings provide an automated quantitative method to examine impacts of interacting multiscale dynamics on AR formation and activities.

Plain Language Summary

Atmospheric Rivers (ARs) are narrow but elongated regions of strong water vapor transport that play a dominant role in cool season precipitation. They are important to local water supply and can also result in extreme environmental and economic damage when the extreme cases hit populated areas, such as the west coast of North America. Their formation and maintenance is the results of a confluence of complex atmospheric phenomena that spans a wide range of spatial and temporal scales, from planetary circulation that occur over weeks, to much more localized (e.g., mesoscale) phenomena that occur over days. This paper seeks to develop a quantitative analysis approach for gaining a better understanding of the complex atmospheric interactions that produce ARs using the recently developed analysis method called the entropy field decomposition (EFD). The EFD is able to characterize the spatial and temporal interactions of multivariate fields and when applied to the wind and specific humidity fields, is shown to automatically detect ARs and characterize their development, maintenance, and structure in two historically important AR events.

1 Introduction

Atmospheric rivers (**ARs**) are long, narrow, and transient corridors of strong water vapor transport, which are the main mechanism to advect moisture to the West Coast of U.S. ((Zhu & Newell, 1998; F. M. Ralph et al., 2004, 2006, 2020)). ARs contribute up to 50% of the annual precipitation over the western U.S. ((Dettinger et al., 2011; Rutz et al., 2014)), which is critical to the water supply. Meanwhile, ARs cause a majority of the major floods over the same region ((F. M. Ralph et al., 2006; Neiman et al., 2011)). Due to the significant social and economic impacts, there has been growing interests and demands in scientific understanding and operational predicting of ARs ((F. M. Ralph et al., 2017, 2020)).

Enhancing our ability to detect, characterize and predict ARs would therefore be of significant societal impact. Complicating this task is the fact that ARs are affected by interacting physical processes on multiple scales, from planetary-scale, synoptic-scale, to mesoscale, such as Rossby wave breaking, extratropical cyclones, low-level jets, and mesoscale frontal waves ((F. M. Ralph et al., 2011; Hu et al., 2017; Zhang et al., 2019; Zhang & Ralph, 2021)). Characterizing the interactions of these multiscale non-linear phenomena that have great impacts on ARs therefore poses a significant data analysis challenge.

In this paper we report our results of an initial investigation of the application of the recently developed *entropy field decomposition* (**EFD**) (Frank & Galinsky, 2016a, 2016b) to this problem. The EFD is a general methodology for estimating and ranking space-time modes of complex, interacting, non-linear systems from noisy data that has proven particularly

useful where exceedingly complex interacting spatially and temporally varying non-linear fields from unique events preclude the use of linear methods or those that require similarity between events via training data. In addition, *space-time information trajectories* (**STIT**) constructed as highest probability pathways through the modes provide a quantitative measure of large scale connectivity. EFD's use of highly relevant prior information embedded *within any individual dataset* facilitates its use in individual unique events. Such is the case in severe local storms where we have previously demonstrated the utility of the EFD approach (Frank et al., 2018). In this paper we present the results of applying EFD to global weather patterns and the question of AR detection using two high-impact AR events in March 2005 and January 2021 over the U.S. West Coast. We demonstrate two main results. First, the EFD modes generated from just the wind field coupled with the specific humidity field are able to accurately detect and rank different modes of the evolution of the ARs. Secondly, the STIT reveal that ARs are coincident with the eastern edge of the trough of amplified Rossby waves, suggesting that the AR activities are closely related to the Rossby waves. These results suggest that EFD provides a unique novel data analysis method with the potential for better understanding of the generation, maintenance, and intensity of ARs.

2 Entropy Field Decomposition

The *Entropy Field Decomposition* (EFD) is a probabilistic method for estimating spatial-temporal modes of complex non-linear systems containing interacting fields (e.g., wind, humidity, temperature, pressure, etc). It is formally based on a field-theoretic mathematical formulation of Bayes' Theorem that enables the hierarchy of multiple orders of field interactions including coupling between fields (Frank & Galinsky, 2016a, 2016b). Its practical utility is enabled by incorporation of the theory of entropy spectrum pathways (ESP) (Frank & Galinsky, 2014) which uses the space-time correlations in each individual dataset to automatically select the very limited number of highly relevant field interactions. There are no training datasets or averages across datasets - just the prior information contained within the single dataset of interest. This method has shown utility in meteorology in the application to severe local storms, in particular tornadic supercells (Frank et al., 2018). In addition to producing estimated field modes, the EFD facilitates the construction of space-time information trajectories (STIT) which are paths of optimal (in the sense of maximum entropy) information within any estimated EFD mode. Multiple connectivity eigenmodes (CEM) generated from each STIT characterize the primary information pathways in the data. The detailed information is provided in Appendix B "Entropy Field Decomposition".

In what follows below, we will denote the calculated k'th EFD mode of the coupled parameters $\alpha_1, \ldots, \alpha_m$ as $\psi^{(k)}_{\alpha_1,\ldots,\alpha_m}(\boldsymbol{x}, t)$. The STIT generated from the modes will be denoted $F^{(k)}_{\alpha_1,\ldots,\alpha_m}(\boldsymbol{x}, t)$. In this paper, the k'th mode was generated by k'th nearest-neighbor in both space and time. However, the algorithm more generally supports indendent variations in coupling $\psi^{(k,l)}$ where $k = 0, \ldots, k_m$ and $l = 0, \ldots, l_n$ represent the coupling length for space and time, respectively, so that an $m \times n$ array of space-time modes with different combinations of space and time scales can be constructed. This provides a refined analysis of spatio-temporal phenomena at different scales and will be pursued in the present context in the future.

2.1 Computational implementation

All the algorithms implemented in this paper were written in standard ANSI C/C++ and parallelized using POSIX threads, resulting in an efficient computational implementation. The computations in the paper of three EFD modes $\psi^{(0,1,2)}$ of wind coupled with specific humidity on the 3.1GB data of size $(nlon, nlat, nlev, nt) = (720, 361, 19, 40)$ took $\approx$ 28 min on a Dual E5-2697 v3 2.6 GHz Fourteen-Core 145W Linux machine with 512GB

DDR4 EEC Registered Memory. STIT and subsequent CEM computations for each mode took approximately 23 min.

3 Data

3.1 Two AR cases

In this study, the EFD analysis on ARs is demonstrated using two selected AR cases: (1) landfalling AR over the U.S. Pacific Northwest on 26th March 2005; (2) landfalling AR over the California coast on 27th January 2021. Both were major landfalling AR events over the West Coast and produced heavy precipitation in the corresponding regions. The March 2005 AR case had a tropical moisture source over the southwest of the Hawaiian Islands, extended northeastward to the U.S. Pacific Northwest, and made landfall over the Washington and north Oregon coast on 26th March with precipitation over 100 mm in the following 24 hours ((F. M. Ralph et al., 2011)). The January 2021 AR case formed on the south side of a deepening extratropical cyclone over the eastern North Pacific, made landfall over the coastal Northern California on 27th January, and then migrated southeastward along the coast of California. This case produced heavy precipitation over a large area of California with a maximum over the Central California and brought severe floodings, which is one of the Billion-Dollar Weather and Climate Disasters in 2021 according to the report from National Oceanic and Atmospheric Administration ((*NOAA National Centers for Environmental Information (NCEI) U.S. Billion-Dollar Weather and Climate Disasters (2022).*, n.d.). These two cases are typical ARs over the eastern North Pacific and the U.S. West Coast, but with some diversities in their characteristics and the large-scale background.

3.2 Data sources

In this study, the Climate Forecast System Reanalysis (CFSR, (Saha et al., 2010)) dataset from the National Centers for Environmental Prediction (NCEP) is used for the analysis of the March 2005 AR case. Since CFSR spans from January 1979 to December 2010, the NCEP Climate Forecast System Version 2 analysis ((Saha et al., 2014)) is used as the extension of CFSR after January 2011 and here for the January 2021 AR case analysis. The CFSR data was obtain on 6-hourly temporal resolution, 0.5° longitude × 0.5° latitude horizontal resolution, and 19 pressure levels (from 1000 hPa to 100 hPa with 50-hPa interval). The variables used in this study include specific humidity (Q), zonal and meridional wind components (U&V), and vertical wind velocity. Vertically integrated water vapor transport (IVT) was calculated using Q and U&V from 1000 hPa to 100 hPa following (Rutz et al., 2014). For each case, an extended period (10 days) of data was utilized to cover the entire life cycle of ARs, starting from 21st March 2005 for the 2005 case and from 22nd January 2021 for the 2021 case, respectively.

4 Results

The EFD modes were calculated over all time frames ($t = 0, 6, 12, \ldots, 234$ hours in steps of 6 hours) spanned from 00 UTZ 21st to 18 UTZ 30th March 2005 for the Jan 2021 event and from 00 UTZ 22nd to 18 UTZ 31st January 2021 for the Mar 2005 event. The results for the Mar 2005 event are shown in Figure 1 and for Jan 2021 in Figure 2. Four key time points in the evolution of the ARs is shown: 1) generation, 2) development, 3) enhancment, and 4) landfall. These correspond to times $t = 72, 96, 120, 144$ for the Mar 2005 event and $t = 48, 72, 96, 120$ for the Jan 2021 event. ARs are often identified and characterized using the integrated vapor transport (IVT), which is shown in the top rows of Figure 1 and Figure 2. In the second row of these figures is shown EFD mode $\psi^{(2)}_{v,q}(\boldsymbol{x}, t)$ (middle panel), the third mode (i.e., k'th nearest neighbors in space and time where $k = 2$.) computed from the (3D+t) wind velocity $v(\boldsymbol{x}, t)$ and specific humidity $q(\boldsymbol{x}, t)$ fields. The bottom rows display the STITs $F^{(2)}_{v,q}(\boldsymbol{x}, t)$ computed for this mode. The wind and specific

humidity at the 850 hPA pressure level from these events are shown at the same time points in Figure A1.

Note that the IVT is an integrated 2D spatial field whereas the EFD is a full 3D spatial field, so provides information as function of altitude. Full volume rendering of this field can be visually confusing, however, so for display purposes, we display the maximum intensity projection (MIP) over all vertical coordinates in Figure 1 and Figure 2 as the EFD modes to compare with the traditional IVT fields. A well-defined AR appeared in the IVT field (top row of Figure 1) at t =72 over the middle North Pacific, where a strong low-level jet captured the water vapor from the southwest of the Hawaiian Island (Figure A1). Then the AR developed and propagated northeastwards in the next two days (t=96 and t=120), until it made landfall over the U.S. Pacific Northwest at t=144. The EFD mode (middle rows in Figures Figure 1 and Figure 2) can reveal the AR through its life cycle, from the genesis stage to landfalling. The EFD modes have been scaled to emphasize their subtle and complex structure. The most intense regions of EFD modes correspond directly to the ARs detected by IVT. It is noteworthy that the EFD mode is calculated using the raw wind and humidity fields directly. It estimates the spatial-temporal modes of the complex non-linear system with the interacting wind and humidity fields, rather than the water vapor transport field (IVT). However, it still can capture the AR patterns, which are very similar to the AR objects in the IVT fields (top and middle rows in Figure 1). It implies that the AR is not only a strong horizontal water vapor transport corrido, but also a region with intense interaction between the wind and water vapor. Different from the 2005 case, the 2021 case formed at the relatively higher latitudes, moved eastward, and made landfall at the California coast (Figures 2 and A2). The EFD modes also revealed the AR patterns, which are similar to the AR objects in the IVT field. These results indicate that the EFD mode can provide an alternative metric to identify ARs based on the interaction between wind and water vapor.

In addition to the EFD mode, the bottom rows of Figures 1 and 2 show the STIT. STITs are high probability pathways through the joint wind-specific humidity EFD mode and is highly related to the upper-level wind field, which could be used to identify Rossby waves. Thus, STITs exhibit a pattern consistent with Rossby waves. Both AR cases are located at the southeast of the wave trough, where the strong low-level southwest wind advects the water vapor from the subtropical/tropical region to the middle latitudes (Figure A1). It indicated that the formation of the two ARs could be highly related to the amplified Rossby wave.

In addition to the main AR cases, EFD also detects a second AR to the East for both cases. While our initial interest was in assessing our ability to detect the major AR events that impacted the US West Coast, the detection of the second AR is important in supporting our hypothesis, derived from the STIT $F^{(2)}_{v,q}(\boldsymbol{x}, t)$ in right hand panels, that the ARs form as a result of convergence along the trough outflow region in what appear to be amplified Rossby waves detected automatically by the STIT. Both second ARs appear in these regions of the Rossby waves. The amplification of the Rossby waves and their relationship to the AR development is evident in the several time frames of the EFD mode $\psi^{(2)}_{v,q}(\boldsymbol{x}, t)$ and STIT $F^{(2)}_{v,q}(\boldsymbol{x}, t)$ for both the Mar 2005 event shown in Figure 1 and for the Jan 2021 event shown in Figure 2, as well as for the two second AR cases.

The volumetric nature of the EFD estimates is emphasized in Figure 3 where slices through $\psi^{(2)}_{v,q}(\boldsymbol{x}, t = 144)$ approximately perpendicular to the primary orientation of the two AR events. The EFD mode exhibits a maximum from the surface to $\approx 800hPa$ for both cases, which indicates that the wind-water vapor interaction is mainly concentrated at the lower levels. This pattern is consistent with the vertical structure of ARs in previous studies based on IVT (e.g., (F. M. Ralph et al., 2011)), showing that the water vapor transport occurs mainly in the troposphere.

5 Discussion and Conclusion

The significant social and economic impact of ARs make their dynamical mechanism and operational prediction of critical importance (F. M. Ralph et al., 2006; F. Ralph, 2020). This in turn necessitates gaining a better understanding of their life cycle - their formation, maintenance, and dissipation. This is complicated as it is now recognized that ARs are complex, multi-scale dynamical events (F. M. Ralph et al., 2011; Zhang et al., 2019) and no current theory for their generation has emerged. Nevertheless, several promising methods have been proposed for their detection and prediction (Guan & Waliser, 2015; Chapman et al., 2019), focussing primarily on spatially localized analysis near the region of AR formation.

In this paper we have developed a different approach that is able to take into account the multiscale, multivariate nature of the atmospheric phenomena that might contribute to AR by use of the entropy field decomposition (EFD). The method can take multiple channels of time-dependent volumes of data as input and examine the influence of interacting fields on the generation of high probability system configurations, or "modes", consistent with the data. In addition, it provides a method for determining high-probability space-time information trajectories (STIT) that reveal large scale connections as a consequence of the interplay of multiscale (planetary, synoptic, and mesoscale) phenomena known to influence AR generation. A critical feature of the EFD method is that reformulation of Bayesian probability theory allows for non-linear interacting fields expected in meteorological application. And given the complexity of individual events, it is a strength of EFD that it uses prior information from within that data itself to determine the most probable modes, rather than requiring training data from other events, which can bias results in favor of average properties, missing important and unique subtleties evident in any individual event. This will become increasingly important as observation methods (radar, satellite, etc) provide ever more detailed information of system dynamics. The EFD thus offers some distinct advantages over existing methods.

This notion is born out by the results of this study, where we have analyzed two very different major AR events, Mar 2005 and Jan 2021. The results, however, demonstrate the EFD is able to detect the ARs automatically directly from an analysis of coupled wind-specific humidity fields. In addition, both events reveal a common large scale dynamical feature of formation along the outflow of the low pressure trough of the Rossby waves, as reveal by the STITs. The STITs formalize the "filamentary structure" highlighted in the earliest AR work of (Zhu & Newell, 1998) and the trajectory analysis (Ryoo et al., 2015). While not the focus of this paper, this method would provide a method for further investigation of the link between ARs and Rossby waves breaking (Ryoo et al., 2013; Hu et al., 2017).

This works suggests that EFD provides a useful new paradigm for detection and quantification of AR's resulting from multiple interacting meteorological fields, and a better understanding of the physics of interacting meteorological fields. On the other hand, this study demonstrates that an AR is not only a strong horizontal water vapor transport corrido, but also a region of intense dynamical interactions of the important meteorological fields (i.e., wind and humidity), which can be detected and quantified with EFD. This leads to the question of EFD's ability to characterize the influence of other large scale phenomena (e.g. MJO) and local phenomena (e.g. orography), and if EFD can provide a new methods for the prediction of ARs. These will be the subject of future work.

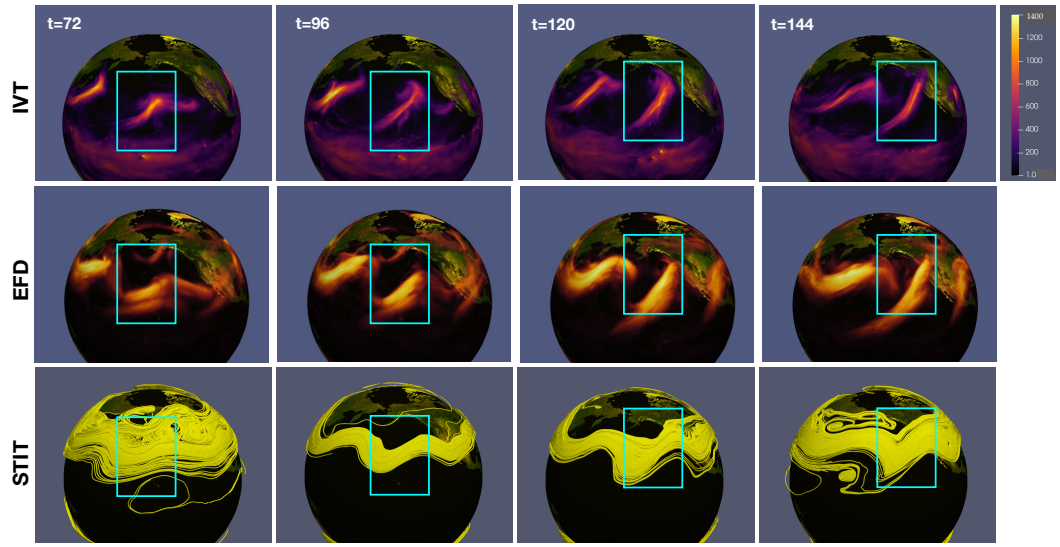

Figure 1. Time evolution of the AR and its relationship to amplification of the Rossby waves for the Mar 2005 event. Time points shown are $t = \{72, 96, 120, 144\}$. (Top row) IVT, (Middle row) Maximum intensity project of the (3D+t) EFD mode $\psi^{(2)}_{v,q}(\boldsymbol{x}, t)$ computed using only the (3D+t) wind field coupled with the (3D+t) specific humidity field, (Bottom row) STITs $F^{(k)}_{\alpha_1,\ldots,\alpha_m}(\boldsymbol{x}, t)$ generated from the EFD mode $\psi^{(2)}$.

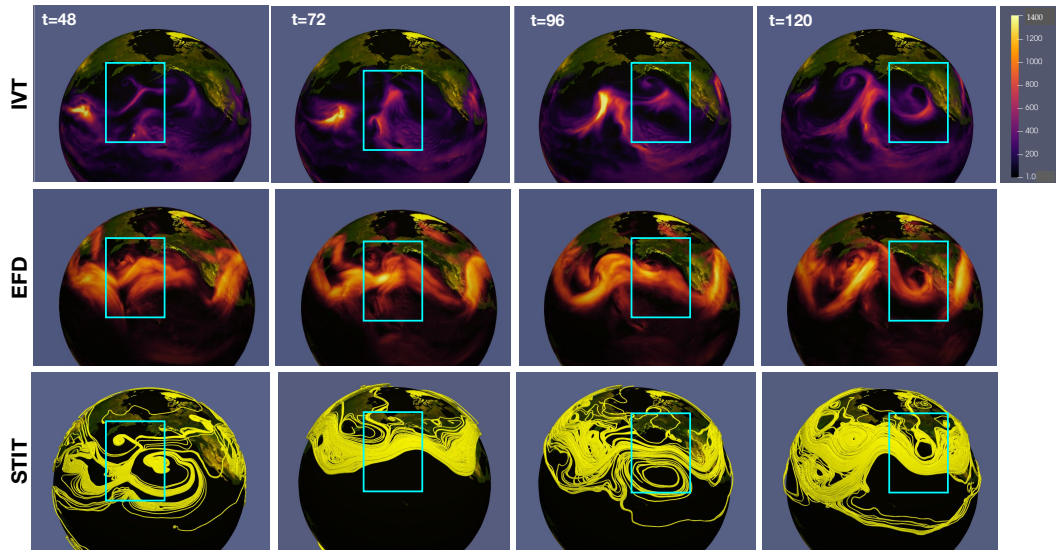

Figure 2. Time evolution of the AR and its relationship to amplification of the Rossby waves for the Jan 2021 event. Time points shown are $t = \{48, 72, 96, 120\}$. (Top row) IVT, (Middle row) Maximum intensity project of the (3D+t) EFD mode $\psi^{(2)}_{v,q}(\boldsymbol{x}, t)$ computed using only the (3D+t) wind field coupled with the (3D+t) specific humidity field, (Bottom row) STITs $F^{(k)}_{\alpha_1,\ldots,\alpha_m}(\boldsymbol{x}, t)$ generated from the EFD mode $\psi^{(2)}$, along with a $\psi^{(2)}$.

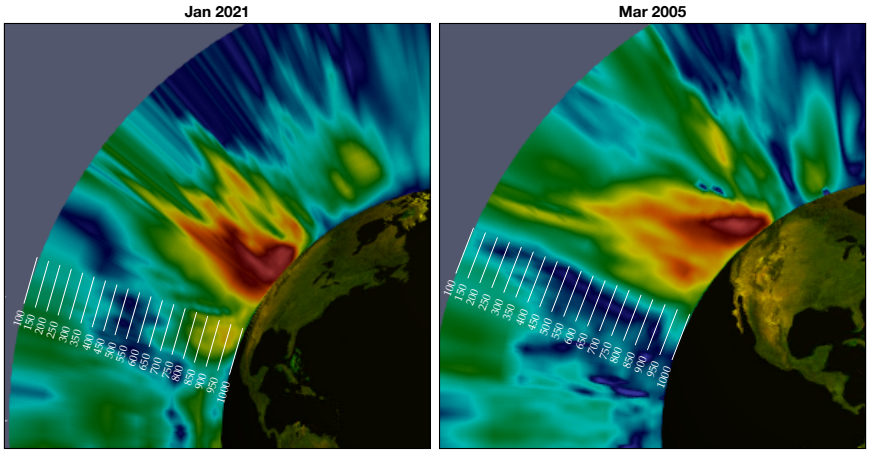

Figure 3. Vertical structure of the EFD mode $\psi^{(2)}_{v,q}(\boldsymbol{x}, t = 144)$ at 122° W over West Coast of the Continental US for the Jan 2021 event (Left) and the Mar 2005 event (Right) emphasized the subtle volumetric variations provided by EFD. The scale of the vertical measurements has been exaggerated by a factor of 10 for visibility, and a different colorscale used.

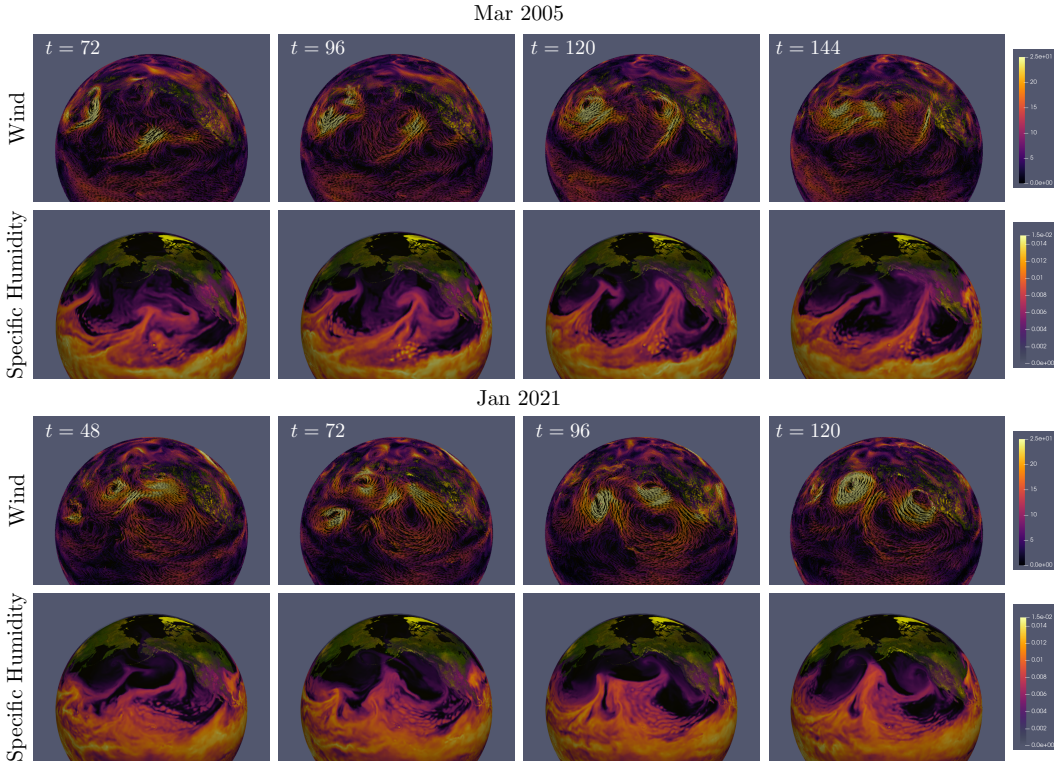

Figure A1. The wind and specific humidity fields at the same time point shown for the EFD results for the Mar 2005 storm (Top) and the Jan 2021 storm (Bottom).

Appendix A Wind and Specific Humidity data

The wind and specific humidity fields at the same time points discussed in the EFD results in Section 4 are shown in Figure A1 for the Mar 2005 event (Top) and the Jan 2021 event (Bottom).

Appendix B Entropy Field Decomposition

B1 Mode estimation

The goal of EFD is to estimate the field $\psi(\boldsymbol{x}, t)$ that describes a continuous (in both space $\boldsymbol{x}$ and time t) parameter space from which the signal s_l are discrete samples of $s_l = \int \psi(\xi)\delta(\xi - \xi_l)d\xi$. This can be done by constructing the posterior distribution of $\psi(\boldsymbol{x}, t)$ given the data d and any prior information I that is available, via Bayes Theorem rexpressed in the language of field theory (Enßlin et al., 2009) as

$$p(\psi|s, I) = \frac{e^{-H(s,\psi)}}{Z(s)} \tag{B1}$$

where $Z(d) = p(d|I) = \int d\psi\, e^{-H(s,\psi)}$ is the *partition function* and $H(s, \psi) = -\ln p(s, \psi|I)$ is the *information Hamiltonian* which takes the form

$$H(s, \psi) = H_0 - j^\dagger \psi + \frac{1}{2}\psi^\dagger D^{-1}\psi + H_i(s, \psi) \tag{B2}$$

where H_0 is a normalizing constant, j and D are the information source and propagator, and † means the complex conjugate transpose. H_i is an interaction term (Enßlin et al., 2009)

$$H_i = \sum_{n=1}^{\infty} \frac{1}{n!} \int \cdots \int \Lambda^{(n)}_{s_1 \cdots s_n} \psi(s_1) \cdots \psi(s_n) ds_1 \cdots ds_n \tag{B3}$$

where $\Lambda^{(n)}_{s_1 \cdots s_n}$ terms describe the interaction strength. In highly complex non-linear systems, j, D, and $\Lambda^{(n)}_{s_1 \cdots s_n}$ are often unknown and too complex for deriving effective and accurate approximations. In this case the ESP method (Frank & Galinsky, 2014), based on the principal of maximum entropy (Jaynes, 1957a, 1957b), provides a general and effective way to introduce powerful prior information to find the most significant contributions to $H(d, \psi)$ by using coupling between different spatio-temporal points that is available from the data itself. This is accomplished by constructing a *coupling matrix* that characterizes the relation between locations i and j in the data $Q_{ij} = e^{-\gamma_{ij}}$ where the γ_{ij} are Lagrange multipliers that describe the relations and depend on some function of the space-time locations i and j. The eigenvalues λ_k and eigenvectors $\phi^{(k)}$ of the coupling matrix Q then define the transition probability from location j to location i of the k'th mode as

$$p_{ijk} = \frac{Q_{ji}}{\lambda_k} \frac{\phi^{(k)}_i}{\phi^{(k)}_j} \tag{B4}$$

For each transition matrix Equation (B4) there is a unique stationary distribution associated with each path k:

$$\mu^{(k)} = \left[\phi^{(k)}\right]^2 \qquad \text{where} \qquad \mu^{(k)}_i = \sum_j \mu^{(k)}_j p_{ijk} \tag{B5}$$

where $\mu^{(1)}$, associated with the largest eigenvalue λ_1, corresponds to the maximum entropy stationary distribution. The essence of the EFD approach (Frank & Galinsky, 2016a, 2016b) is to incorporate these coupling matrix priors into the information Hamiltonian Equation (B2) by expanding the signal $s(\boldsymbol{x}, t)$ into a Fourier expansion using $\{\phi^{(k)}\}$ as the basis functions which allows expressing the information Hamiltonian Equation (B2) in this ESP basis as

$$H(d, a_k) = -j^{\dagger}_k a_k + \frac{1}{2} a^{\dagger}_k \Lambda a_k + \sum_{n=1}^{\infty} \frac{1}{n!} \sum_{k_1}^{K} \cdots \sum_{k_n}^{K} \tilde{\Lambda}^{(n)}_{k_1 \cdots k_n} a_{k_1} \cdots a_{k_n} \tag{B6}$$

where matrix Λ is the diagonal matrix $\mathrm{Diag}\{\lambda_1, ..., \lambda_K\}$, composed of the eigenvalues of the coupling matrix, and $j_k = \int j \, \phi^{(k)} ds$ is the amplitude of kth mode in the expansion of the source j and the new interaction terms $\tilde{\Lambda}^{(n)}$ is the original interaction term projected onto the ESP basis functions. From this can be derived a very simple expression for the solution for the amplitudes a_k through the eigenvalues and eigenvectors of coupling matrix (Frank & Galinsky, 2016a, 2016b). This can be extended to incorporate coupling between different parameters as well (Galinsky & Frank, 2017).

B2 Space-Time Information Trajectories

Space-time information trajectories are defined as streamlines generated using the global path entropy change

$$S_i = -\sum_k \mu^{(k)} \sum_j p_{ijk} \ln p_{ijk} \tag{B7}$$

where the equilibrium μ distributions and transitional probabilities p_{ij} were obtained from the space-time nearest neighbor coupling matrix $Q^F_{ij}(t_0) = \mathcal{R}^m_{ij} d(x_i, t_0) d(x_j, t_0)$ where $\mathcal{R}_{ij}$ is either the mean or maximum of the temporal pair correlation function computed for spa-

tial nearest neighbors i and j, $\phi^{(1)}(x_j, t_0)$ is the eigenmodes that corresponds to the largest eigenvalue of $Q(x_i, x_j, t_0)$, and the exponent $m \geq 0$ is used to attenuate the importance of correlations. The global entropy field Equation (B7) was obtained under the Markovian assumption in the limit of long pathway lengths (or large times) (Shannon, 1948; McMillan, 1953) and describes the global flow of information. The trajectories are generated by linearizing the Fokker-Planck equation with a potential in the form of the global entropy Equation (B7) (Frank & Galinsky, 2014) and finding the characteristics solution using the Hamiltonian set of equations to construct the space-time trajectories are generated using a geometric-optics based approach, as described in (Galinsky & Frank, 2015).

Acronyms

NCEP National Centers for Environmental Prediction
EFD Entropy field decomposition
STIT Space-time information trajectory
ESP Entropy spectrum pathways

Open Research

The NCEP Climate Forecast System Reanalysis data (CFSR) used in this study is accessible from NCAR's Research Data Archive https://rda.ucar.edu/datasets/ds093.0/ and Climate Forecast System Version 2 analysis data (CFSv2) is accessible from NCAR's Research Data Archive https://rda.ucar.edu/datasets/ds094.0/. Figures were made with Paraview version 5.10.0 (Kitware Inc., 2007) available under an open BSD license at https://www.paraview.org. The computational software associated with this manuscript is licensed under UCSD and is available upon request to lfrank@ucsd.edu.

Acknowledgments

LRF and VLG were supported by NSF grant ACI-1550405. ZZ and MR were supported by the U.S. Army Corps of Engineers "Forecast-Informed Reservoir Operations" Program and the California Department of Water Resources "Atmospheric Rivers Program."

References

Chapman, W. E., Subramanian, A. C., Delle Monache, L., Xie, S. P., & Ralph, F. M. (2019). Improving Atmospheric River Forecasts With Machine Learning. *Geophys. Res. Lett*, *46*(17-18), 10627–10635.

Dettinger, M. D., Ralph, F. M., Das, T., Neiman, P. J., & Cayan, D. R. (2011). Atmospheric rivers, floods and the water resources of california. *Water*, *3*(2), 445–478.

Enßlin, T. A., Frommert, M., & Kitaura, F. S. (2009). Information field theory for cosmological perturbation reconstruction and nonlinear signal analysis. *Phys. Rev. D*, *80*(10), 105005.

Frank, L. R., & Galinsky, V. L. (2014). Information pathways in a disordered lattice. *Phys. Rev. E*, *89*(3), 11.

Frank, L. R., & Galinsky, V. L. (2016a). Detecting spatio-temporal modes in multivariate data by entropy field decomposition. *J. Phys. A*, *49*, 395001.

Frank, L. R., & Galinsky, V. L. (2016b). Dynamic multi-scale modes of resting state brain activity detected by entropy field decomposition. *Neural Comput.*, *28*(9), 1769–1811.

Frank, L. R., Galinsky, V. L., Orf, L., & Wurman, J. M. (2018). Dynamic multiscale modes of severe storm structure detected in mobile doppler radar data by entropy field decomposition. *J. Atmos. Sci.*, *75*, 709-730.

Galinsky, V. L., & Frank, L. R. (2015, May). Simultaneous multi-scale diffusion estimation and tractography guided by entropy spectrum pathways. *IEEE Trans. Med. Imag.*, *34*(5), 1177-1193.

Galinsky, V. L., & Frank, L. R. (2017). A unified theory of neuro-MRI data shows scale–free nature of connectivity modes. *Neural Computation*, *29*, 1441-1467.

Guan, B., & Waliser, D. E. (2015). Detection of atmospheric rivers: Evaluation and application of an algorithm for global studies. *Journal of Geophysical Research-Atmospheres*, *120*(24), 12514–12535.

Hu, H., Dominguez, F., Wang, Z., Lavers, D. A., Zhang, G., & Ralph, F. M. (2017, May). Linking Atmospheric River Hydrological Impacts on the U.S. West Coast to Rossby Wave Breaking. *Journal of Climate*, *30*(9), 3381–3399.

Jaynes, E. T. (1957a). Information Theory and Statistical Mechanics. *Phys. Rev.*, *106*(4), 620–630.

Jaynes, E. T. (1957b). Information theory and statistical mechanics. II. *Phys. Rev.*, *108*(2), 171.

Kitware Inc. (2007). *ParaView Guide, A Parallel Visualization Application.* `https://www.paraview.org`.

McMillan, B. (1953). The basic theorems of information theory. *Ann. Math. Stat.*, *24*(2), 196–219.

Neiman, P. J., Schick, L. J., Ralph, F. M., Hughes, M., & Wick, G. A. (2011, December). Flooding in Western Washington: The Connection to Atmospheric Rivers. *Journal of Hydrometeorology*, *12*(6), 1337–1358.

NOAA National Centers for Environmental Information (NCEI) U.S. Billion-Dollar Weather and Climate Disasters (2022). (n.d.). `https://www.ncei.noaa.gov/access/billions/`.

Ralph, F. (2020). *Atmospheric rivers* (1st ed.; F. Ralph, M. Dettinger, J. Rutz, & D. Waliser, Eds.). Springer.

Ralph, F. M., Cannon, F., Tallapragada, V., Davis, C. A., Doyle, J. D., Pappenberger, F., … Monache, L. D. (2020). West coast forecast challenges and development of atmospheric river reconnaissance. *Bulletin of the American Meteorological Society*, *101*(8), E1357 - E1377.

Ralph, F. M., Dettinger, M., Lavers, D., Gorodetskaya, I. V., Martin, A., Viale, M., … Cordeira, J. (2017). Atmospheric rivers emerge as a global science and applications focus. *Bulletin of the American Meteorological Society*, *98*(9), 1969 - 1973.

Ralph, F. M., Neiman, P. J., Kiladis, G. N., Weickmann, K., & Reynolds, D. W. (2011, April). A Multiscale Observational Case Study of a Pacific Atmospheric River Exhibiting

Tropical-Extratropical Connections and a Mesoscale Frontal Wave. *Monthly Weather Review*, *139*(4), 1169–1189.

Ralph, F. M., Neiman, P. J., & Wick, G. A. (2004, July). Satellite and CALJET Aircraft Observations of Atmospheric Rivers over the Eastern North Pacific Ocean during the Winter of 1997/98. *Monthly Weather Review*, *132*, 1721–1745.

Ralph, F. M., Neiman, P. J., Wick, G. A., Gutman, S. I., Dettinger, M. D., Cayan, D. R., & White, A. B. (2006). Flooding on California's Russian River: Role of atmospheric rivers. *Geophys. Res. Lett*, *33*(13).

Rutz, J. J., Steenburgh, W. J., & Ralph, F. M. (2014, February). Climatological Characteristics of Atmospheric Rivers and Their Inland Penetration over the Western United States. *Monthly Weather Review*, *142*, 905–921.

Ryoo, J.-M., Kaspi, Y., Waugh, D. W., Kiladis, G. N., Waliser, D. E., Fetzer, E. J., & Kim, J. (2013, September). Impact of Rossby Wave Breaking on U.S. West Coast Winter Precipitation during ENSO Events. *Journal of Climate*, *26*(17), 6360–6382.

Ryoo, J.-M., Waliser, D. E., Waugh, D. W., Wong, S., Fetzer, E. J., & Fung, I. (2015). Classification of atmospheric river events on the US West Coast using a trajectory model. *Journal of Geophysical Research-Atmospheres*, *120*(8), 3007–3028.

Saha, S., Moorthi, S., Pan, H.-L., Wu, X., Wang, J., Nadiga, S., … Goldberg, M. (2010). The ncep climate forecast system reanalysis. *Bulletin of the American Meteorological Society*, *91*(8), 1015 - 1058.

Saha, S., Moorthi, S., Wu, X., Wang, J., Nadiga, S., Tripp, P., … Becker, E. (2014). The ncep climate forecast system version 2. *Journal of Climate*, *27*(6), 2185 - 2208.

Shannon, C. (1948). A mathematical theory of communication. *Bell Syst. Tech. J.*, *27*, 379–423, 623–656.

Zhang, Z., & Ralph, F. M. (2021, May). The Influence of Antecedent Atmospheric River Conditions on Extratropical Cyclogenesis. *Monthly Weather Review*, *149*(5), 1337–1357.

Zhang, Z., Ralph, F. M., & Zheng, M. (2019). The Relationship Between Extratropical Cyclone Strength and Atmospheric River Intensity and Position. *Geophys. Res. Lett*, *46*(3), 1814–1823.

Zhu, Y., & Newell, R. E. (1998, March). A Proposed Algorithm for Moisture Fluxes from Atmospheric Rivers. *Monthly Weather Review*, *126*, 725–735.